Journal of
Water & Climate Change

IWA PUBLISHING

Journal of Water and Climate Change Vol 14 No 8, 2755 doi: 10.2166/wcc.2023.103

Mass transfer process in the removal of Congo Red (CR) onto Natural Clay (NC): Kinetic, isotherm modeling, and thermodynamic study

Moussa Abbas[a,*] and Mohamed Trari[b]

[a] Laboratory of Applied Chemistry and Materials (LabCAM), University of M'hamed Bougara of Boumerdes, Avenue de l'Indépendance, Boumerdes, 35000, Algeria
[b] Laboratory of Storage and Valorization of Renewable Energies, Faculty of Chemistry (USTHB), Algiers BP 32-16111, Algeria
*Corresponding author. E-mail: m.abbas@univ-boumerdes.dz

ABSTRACT

Industrial growth and technological advancement have led to the worldwide introduction of pollutants of diverse nature into water bodies including pollutants such as dyes and organic contaminants. Their presence in industrial effluents or drinking water is a public health problem. The aim of this study was to evaluate the adsorption of Congo Red (CR) onto Natural Clay (NC) realized in a batch system. The effects of contact time, initial pH, stirring speed, temperature, adsorbent dose, and initial CR concentration on the adsorption capacity were investigated. The NC was characterized by the FTIR, DRX, BET, and point of zero charge. The experimental isotherm data follow well the Langmuir equation, providing a better fit of the equilibrium adsorption data. Under optimized conditions, up to 212.766 mg/g at 25 °C is removed from the solution. The adsorptions kinetics were found to follow rather a pseudo second-order kinetic model with a determination coefficient (R^2) of 0.999. The adsorption isotherms at different temperatures have been used for the determination of thermodynamic parameters, i.e., the negative free energy ΔG^0 (10.081 to 1.087 kJ/mol), positive enthalpy change ΔH^0 Q5 (64 = 175 kJ/mol) values indicate that the overall CR adsorption is spontaneous and endothermic in nature.

Key words: adsorption, Congo Red, kinetics, modeling, Natural Clay, thermodynamic

HIGHLIGHTS

- The aim of this study was to evaluate the adsorption of Congo Red onto Natural Clay (NC).
- The effects of parameters were investigated graphically.
- Under optimized conditions, up to 212.766 mg/g at 25 °C is removed from the solution.
- The adsorption kinetics were found to follow rather a pseudo-second-order kinetic model.
- The thermodynamic parameters indicate the adsorption is spontaneous and endothermic in nature.

GRAPHICAL ABSTRACT

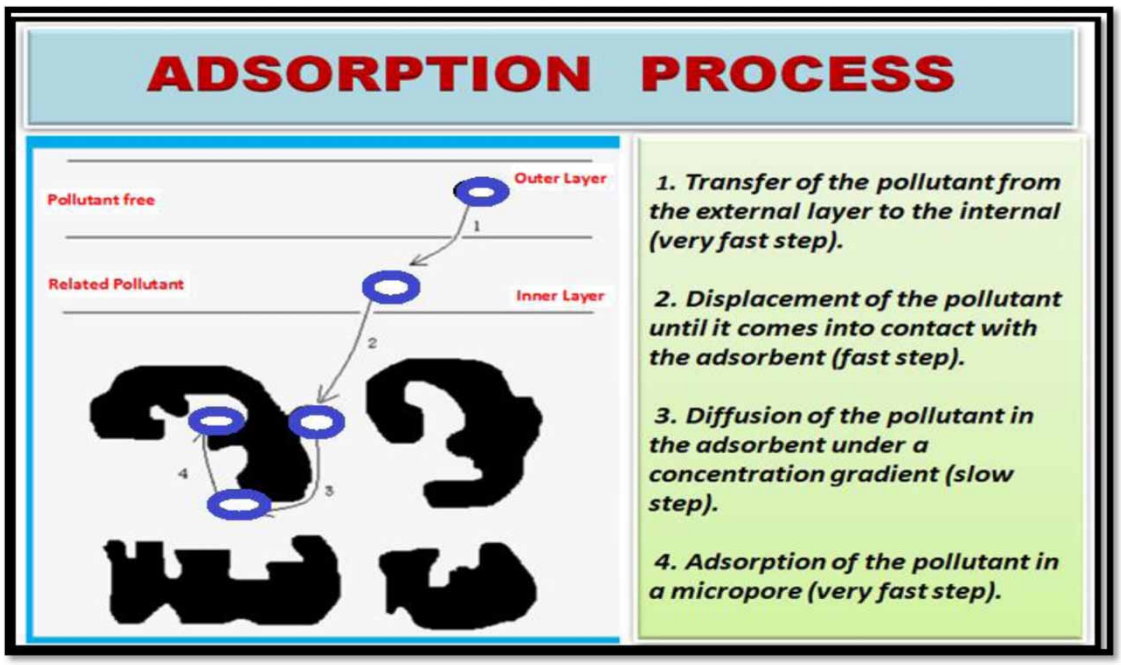

1. INTRODUCTION

Global climate change and population growth have put pressure on water supplies. Wastewater management and potable water purification are crucial in supporting the rapid development of human society and mitigating environmental pollution and health risks. One of the major problems with wastewater is colored effluent. Discharges from different industries such as textile industries, cosmetics, paper and printing, rubber, leather, pharmaceuticals, food, leather tanning, paint manufacturing, battery manufacturing industries, and plastic industries contain many toxic pollutants, such as dyes, which harm the environment (Yu *et al.* 2021). There are more than 100,000 types of dyes commercially available, with more than 7×10^5 tons of dyes tuff produced annually (Nasuha & Hameed 2011). Dyes can be classified into two categories: non-ionic (vat and disperse dyes) and ionic, i.e. cationic (basic) and anionic (reactive, direct and acidic) (Homaeigohar 2020). The presence of dyes in aquatic ecosystems reduces light penetration and thus decreases the photosynthesis necessary for living organisms (Krishna Moorthy *et al.* 2021). In addition, industrial dyes are mutagenic, toxic, and dangerous to both humans and animals (Ismail *et al.* 2022). Congo Red (CR) is a benzidine-based dye with two molecules of naphthenic acid and the first synthetic dye capable of directly dyeing cotton. It is very sensitive to acids and its color changes from red to blue in the presence of inorganic acids; this dye is known to metabolize benzidine, a known human carcinogen (Mall *et al.* 2005). Therefore, the removal of dyes from aquatic environments is a necessary process to prevent water pollution (Omar *et al.* 2018). In this regard, several processes, including mechanical (filtration and reverse osmosis), physical (adsorption, extraction and flocculation), chemical (precipitation, oxidation, ion exchange, ozonolysis), and thermal (evaporation and distillation) have been used to remediate water contaminated with dyes (Abbas *et al.* 2019; Abbas & Trari 2020a, 2020b). However, these methods have certain drawbacks such as high cost, secondary pollution, low efficiency and are not effective on a large scale (remediation of polluted soil) (Chen *et al.* 2015). Therefore, bioremediation using microbial species is a low-cost alternative with environmentally friendly characteristics (Elnahas *et al.* 2021). The adsorption is an attractive method for the removal of dyes due to its low maintenance, simple operation and removal effectiveness, especially if the adsorbent is inexpensive and readily available. In this regard, activated carbon (AC) is a versatile adsorbent used regularly for the adsorption process, but remains relatively expensive. Therefore, many researchers have used different wastes for the development of activated carbons (AC) at low economic cost, this allowed us to eliminate them from the natural environment and recover them for water treatment. Therefore, this has prompted a growing research interest in the production of ACs from renewable and cheaper precursors which are mainly industrial and agricultural by-products, for the wastewater treatment. However, the available ACs in commerce are

relatively expensive, their production and regeneration cost constitute limiting factors. Hence, most researchers worldwide have focused on the search of new low-cost precursors especially issued from agricultural wastes. The adsorbent used in the present case is Natural Clay (NC) and this study was carried out with the aim to optimize conditions such as initial dye concentration (C_0), pH, contact time, adsorbent dosage, agitation speed, and temperature. In addition, the equilibrium adsorption data were fitted to various equations in order to obtain the constants related to the adsorption phenomena. Equilibrium and kinetic analysis were conducted to determine the factors controlling the adsorption rate, the optimization of various parameters in the dye recovery and to find out the possibility of using this material as low-cost adsorbent for dye removal.

2. MATERIALS AND METHODS

2.1. Equipment

- The spectrophotometry is a technique which owes its development to progress in the quantum mechanics allowing, among other things, to identify a chemical substance and to determine the concentration of a solute in solution, by using the Beer–Lambert's law.
- The pH of the solutions was accurately measured using a microprocessor-based pH meter of the HANNA HI 8521 type. The instrument was calibrated with commercial buffers of pH values 4, 7, and 10. The pH was adjusted to by using H_2SO_4 and NaOH, respectively, for acidic and basic media.
- The FTIR spectroscopy was used to identify the characteristic functional groups of commercial clay. Five mg of NC were mixed with spectroscopic grade dry KBr and pressed under 4,500 psi pressure to form a thin disc. Then, the FTIR spectra were plotted with a Perkin Elmer 2000 infrared spectrometer in the range (4,000–400 cm^{-1}) for 16 times to increase the signal-to-noise ratio.
- The surface area of the sample clay was determined by the BET method using a AsiQuin, Automated Gas Sorption Analyser Quantachrome Instrument Version 2.02. The specific surface area and pore structure of ACs were characterized by N_2 adsorption–desorption isotherms at −196 °C using the ASAP 2010 Micromeritics equipment.
- The X-ray diffraction (XRD) patterns of NC was obtained with a Philips X-ray diffractometer (PW 1890 model) operating at 40 kV, 40 mA and equipped with $Cu_{K\alpha}$ radiation ($\lambda = 1.54$ Å). The patterns were obtained with CONIT T-2 T scan mode at 0.17°/step of step width and 8°/min of scan speed.
- The chemical analysis was performed by the X-ray fluorescence (XRF) using Horiba XRF
- The Zero Point Charge $pH_{(zpc)}$ of the NC, i.e., the pH for which the surface charge is zero, is obtained using a procedure similar to that reported elsewhere (Abbas 2021). Briefly, 20 mL of of KNO_3 solutions (0.01 M) were placed in closed conical flasks; the pH of each solution was adjusted between 2 and 14 by addition of HCl or NaOH solution. Then, 0.1 g of CC was added and the final pH was measured after 24 h under magnetic stirring at ambient temperature; $pH_{(zpc)}$ is the final pH versus initial pH crosses the line at final pH = initial pH.

2.2. Materials

The anionic dye used as adsorbate is CR purchased from the Nizochem Laboratory, with a formula $C_{32}H_{22}N_6Na_2O_6S_2$ and a molecular weight of 696.66 g/mol, respectively (Table 1). One hundred mg/L of solution was prepared by adding 0.1 g of CR in 1,000 mL of distilled water, and solutions required for the experimental study were prepared by diluting the CR stock solution to various initial adsorbate concentrations. The adsorbent used in this study is NC, provided by the edible oil refining unit (Algeria).

2.3. Adsorption experiments

The effects of the initial CR concentration C_0 (20–80 mg/L), solution pH (1–12), adsorbent dose (10–50 g/L), agitation speed (100–700 rpm), and temperature (298–338 K) on the CR adsorption were studied in batch mode between 0 and 60 min. For the kinetic studies, desired quantities of NC were contacted with 100 mL of CR solutions in Erlenmeyer flasks, placed on a rotary shaker at 400 rpm; the aliquots were taken at regular time intervals and vigorously centrifuged (6,000 rpm, 15 min) to separate the solid phases from the liquid. The remaining CR concentration was titrated with a UV–visible spectrophotometer (Perkin Elmer model 550S) at $\lambda_{max} = 494$ nm (Figure 1) and deduced by linear interpolation. The adsorbed quantity q_t (mg/g)

Table 1 | General characteristics of Congo Red

Physical and chemical properties		Chemical structure
Brute formula	$C_{32}H_{22}N_6Na_2O_6S_2$	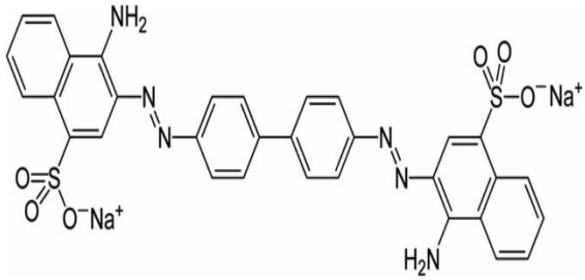
Molecular weight	(696.663 ± 0.004) g/mol	
pKa	4	
Composition (%)	C: 55.0, N: 12.06, O: 13.78	
	H: 3.18, Na: 6.60, S: 9.21	
Wavenumber (λ_{max})	494 nm	
Name	Congo Red	
Melting temperature	360 °C	
Boiling pressure	760 mm Hg	
Solubility in water	25 g/L at $T = 20$ °C	
Solubility in alcohol	Very soluble	

Figure 1 | UV–visible spectrum of Congo Red (CR).

of CR elimination by NC is calculated from the following equation:

$$q_t = \frac{(C_0 - C_t) \times V}{m} \quad (1)$$

C_t is the CR concentrations (mg/L) at time (t), V the volume of solution (L) and m the mass of NC (g).

3. RESULTS AND DISCUSSION

3.1. Characterization of the adsorbent (NC)

3.1.1. Analyses of the NC composition

The XRF was performed to determine the chemical composition of the adsorbent. The content of elements present in NC and the main mineralogical constituents are silica and alumina, thus confirming the presence of Si, Al, Mg, Fe, K, Ca and Na.

These results corroborate the XRF analysis, which indicates the presence of these elements in oxides: SiO_2 (53.4% in mass), Al_2O_3 (4%), Fe_2O_3 (1.5%), MgO (30.5%), Na_2O (0.3%), CaO (0.7%), and K_2O (1%). The loss on ignition at 1,000 °C of this material is 8.5%.

3.1.2. Analyses of the NC surface chemical

The infrared analysis spectrum was carried out in transmittance mode using FTIR spectrophotometer between 4,000 and 400 cm^{-1}. The analysis was done directly on the clay powder and the recorded spectrum is shown in Figure 2. Examination of the infrared spectrum revealed absorption bands that we present as follows: The band centered at 3,678 cm^{-1} is attributed to the stretching vibrations of the –OH group bonded to the Mg cation (Mg_3OH stretching) (Takhashi *et al.* 1994). This peak confirms the character trioctahedral of the different clay minerals that make up clay (kerolite, steven site, and sepiolite). The bands at 3,430 and 1,637 cm^{-1} are attributed to the deformation vibrations of H_2O adsorbed between the sheets (Yeniyol 2020). The intense band centered at 1,016 cm^{-1} is assigned to the elongation vibrations of the groups Si–O of Q sites (Brew & Glasser 2005). The bands 669 and 473 cm^{-1} are characteristic of Si–O–R vibrations (R = Mg, Fe, or Al) (Christidis & Mitsis 2006). The band at 1,417 cm^{-1} is due to the presence of a small amount of calcite in the mixture (Matei *et al.* 2020).

3.1.3. Analyses of the NC composition

XRD was used to determine the different mineralogical phases that constitute the NC; the diffractogram obtained is shown in Figure 3. The different phases that constitute this clay are mainly the kerolite-stevensite type, composed of 98% clay minerals. The main crystalline phases present on the diffractogram are as follows: sepiolite (S) ($2\theta = 7.1°$), clay minerals ($2\theta = 19.5°$), calcite ($2\theta = 29.4°$; 36°, 43.1° and 60.5), and quartz at $2\theta = 26.4°$, 52.8°, and 71.8°.

3.1.4. Textural properties

Textural measurements of the adsorbent were made from the N_2 adsorption isotherm (Figure 4). The adsorption/desorption isotherm is obtained by the continuous introduction of known quantities of nitrogen at the boiling point of liquid nitrogen (77 K) and under atmospheric pressure. The quantity of gas adsorbed or desorbed is then determined as a function of the equilibrium pressure. The isotherm obtained gives access to the specific surface of the sample determined according to

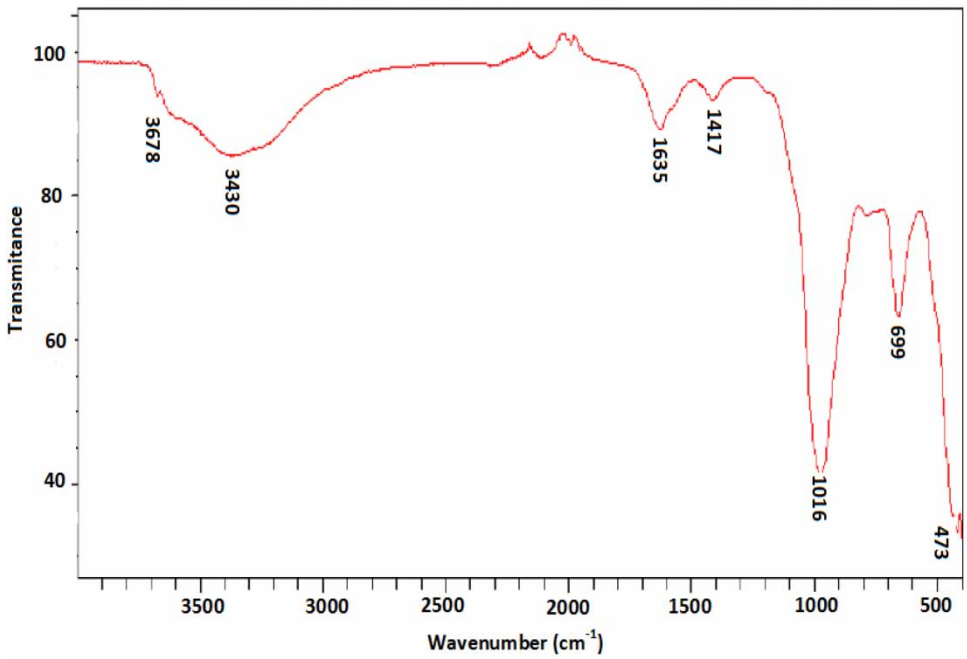

Figure 2 | Infrared spectrum of Natural Clay (NC).

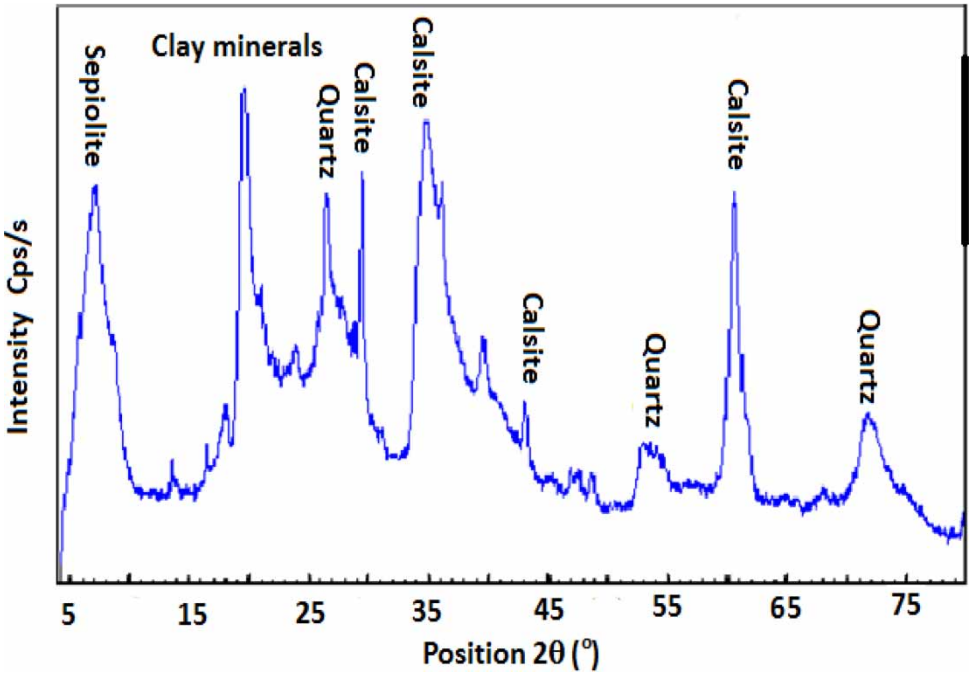

Figure 3 | Diffraction spectrum of Natural Clay (NC).

various mathematical expressions BET, Dubinin–Radushkevich (D–R) model, BET specific surface ($S_{BET} = 207\ m^2/g$), microporous specific volume ($V_{mic} = 0.05\ cm^3/g$), external specific surface ($S_{ext} = 139\ m^2/g$), microporous specific surface ($S_{mic} = 49\ m^2/g$), and the total specific surface ($S_{Tot} = 188\ m^2/g$).

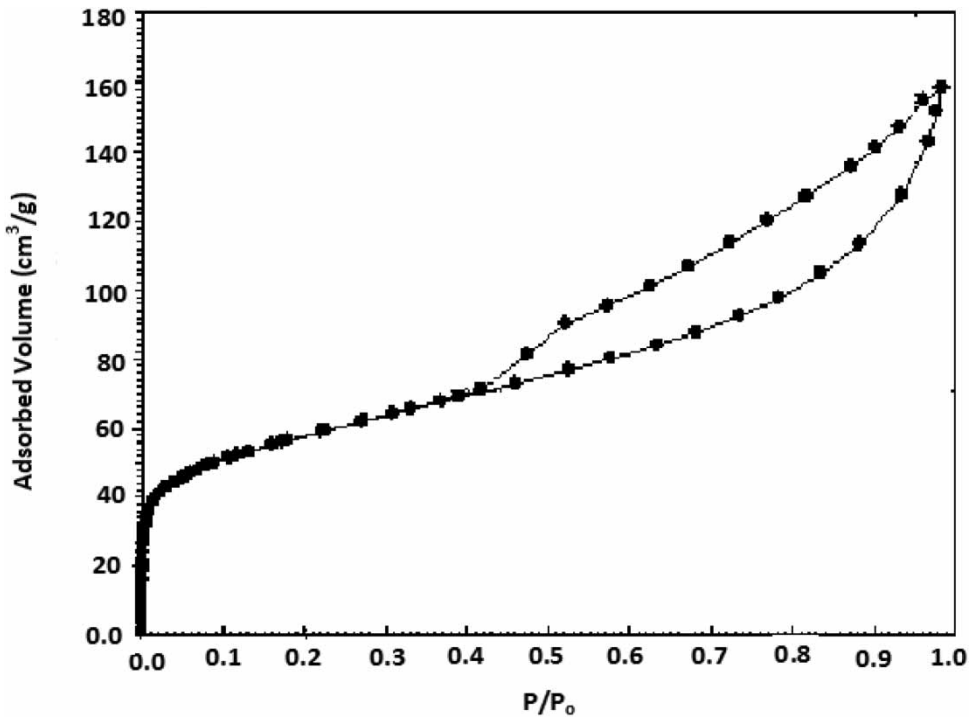

Figure 4 | Adsorption and desorption isotherms of nitrogen at 77 K by NC.

3.2. Studies of the effect of process variables

3.2.1. Point of Zero Charge (pH_{pzc}) and effect of pH

The pH effect on the CR adsorption onto NC can be explained from the zero point charge (pH_{pzc}), the surface functions of the material have a significant influence on the adsorption performance (Reddad *et al.* 2002). The basic or acidic nature of the adsorbent surface governs its retention capacity vis-à-vis to the pollutant. However, the character and chemical properties of adsorbent are directly linked to the nature of the functional groups located on its surface. The surface charge of the adsorbent, resulting from the acid–base equilibrium can be positive or negative depending on the environmental conditions. Therefore, an important feature of the surface is the determination of $pH_{pzc} = 7.65$ (Figure 5) by the drift method which defines the pH for which the surface charge, linked to the exchange of protons, cancels out; pH_{pzc} characterizes the acidity or alkalinity of the surface. Below pH_{pzc}, the surface positively charged (acidity) where oxygen groups are in the cationic form, which converts to negative above pHpzc (alkalinity) and tends to decrease when the oxygen content increases. Figure 6 shows that the amount of RC adsorbed decreases with increasing pH.

According to the results of determining pHpzc of clay, the surface of our adsorbent acquires a positive charge in an acidic medium by absorbing H^+ ions, and adsorbs the RC negatively charged due to the sulfonated group by electrostatic attraction, which leads to greater adsorption capacity of clay. On the other hand, in a basic medium ($pH > 8$), the clay surface is negatively charged by absorbing OH^- ions and can reject the negatively charged RC due to the sulfonated group by electrostatic repulsion, resulting in lower adsorption capacity of the clay (Yandri *et al.* 2023). The plateau observed between pH 7 and 8, can be explained by the fact that the surface of our adsorbent is neutral in this area (pHpzc of clay corresponds to a pH between 7 and 8).

3.2.2. Effect of contact time and initial concentration of CR

The examination of Figure 7 shows that the adsorption capacity of CR onto NC increases with increasing contact time until saturation where no CR molecule can be retained; the maximal adsorption is reached after 40 min, which corresponds to the equilibrium time.

(i) It is noted that when the CR concentration C_0 increases from 20 to 80 mg/L, the adsorbed quantity increases from 18.44 to 72.83 mg/g, resulting from attractive electrostatic forces between the adsorbent/pollutant, the same result was observed

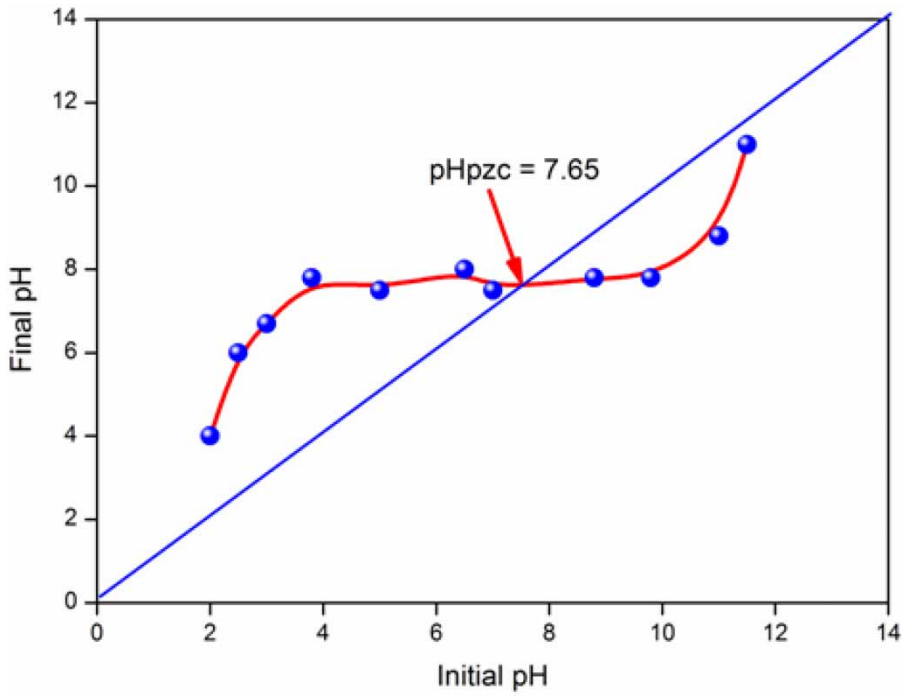

Figure 5 | Determination of the isoelectric pH of Natural Clay.

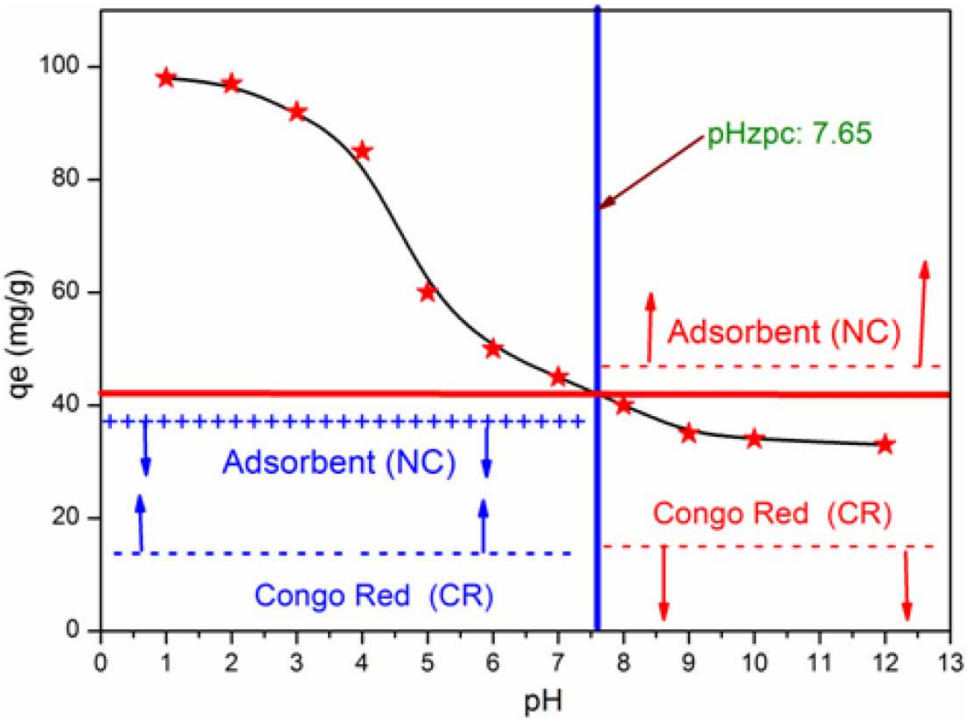

Figure 6 | Influence of the pH on the amount of adsorption of CR onto CN ($C_i = 100$ mg/L, adsorbent dose = 1 g/L, agitation speed $V =$ 300 rpm, $T = 25$ °C, and $t = 60$ min).

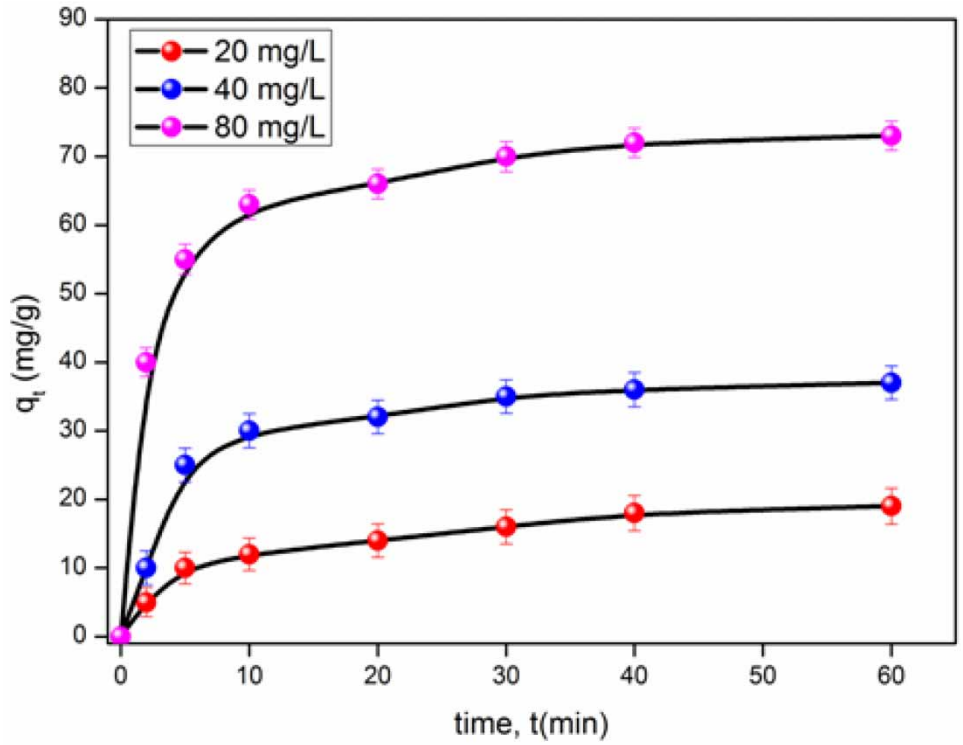

Figure 7 | Influence of time and concentration of CR on the amount of adsorption (pH = 7, adsorbent dose = 1 g/L, agitation speed $V =$ 300 rpm, and $T = 25$ °C).

elsewhere (Abbas 2020, 2022; Abbas *et al.* 2020). This is due to the increased driving force which comes from the concentrations gradient with increasing CR concentration that overcomes the resistance to the mass transfer of CR ions between the liquid and solid phases. Fast CR adsorption is due to the presence of free sites on the adsorbent surface, which reflects the linear increase of the adsorption capacity with time in the range 0–20 min.

(ii) Reduction of the adsorption rate in the range 20–40 min reflected by a small increase in the adsorption capacity attributed to the decrease in the CR concentration C_0 and the number of available sites of NC.

(iii) Stability of the adsorption capacity is observed in the range 40–60 min, due to the total occupation of adsorption sites: the establishment of the level therefore reflects this stage. These results clearly indicate that if the CR concentration in solution is high, there are more molecules which diffuse toward the surface of available sites onto NC, resulting in a significant increase in the CR retention.

3.2.3. Effect of agitation speed

The influence of stirring speed on the adsorption capacity of RC on NC was studied by bringing 100 mL of a solution of RC ($C_0 = 100$ mg/L) into contact with 0 and 1 g of clay at a temperature of 25 °C at different stirring speeds ranging from 0 to 700 rpm (Figure 8). Examination of this figure reveals that the amount of adsorbed RC increases with the stirring speed in the row (100–600 rpm) but the adsorbed amount remains practically constant in the range 600–700 rpm. It should be noted that the test without agitation did not lead to adsorption, probably due to an incomplete dispersion of the particles of the adsorbent. This result in an agglomeration of these particles and therefore a reduction in the contact surface/adsorbent; the adsorbate induces an increase in the resistance to mass transfer inside the liquid–solid interface. For this, it is preferable to carry out the adsorption tests under magnetic stirring; the speed of 600 rpm is retained for the rest of the adsorption tests.

3.2.4. Effect of adsorbent dosage

The influence of the adsorbent dose on the amount of RC adsorbed was studied by bringing the dye solution into contact at an initial concentration C_0 of 100 mg/L with an adsorbent dose which varies from 0.1 to 0.5 g; the results are illustrated in

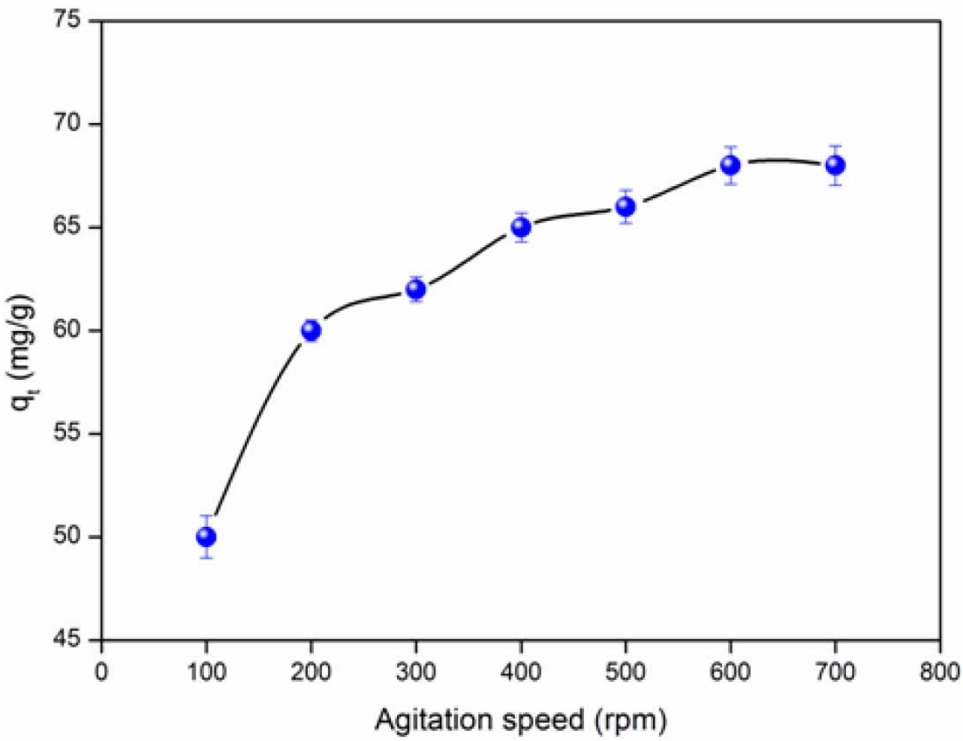

Figure 8 | Influence of the stirring speed on the amount of adsorption of RC onto NC (C_i =100 mg/L, adsorbent dose = 1 g/L, pH = 2, T = 25 °C, and t = 60 min).

Figure 9. The curve clearly reveals that the adsorbed quantity decreases with increasing the NC dose. This can be explained by the fact that many effective and active sites are used at higher doses due to the aggregation and overlapping of adsorbent particles in the solution, resulting in a decrease of the surface area of absorption accessible by RC molecules. This result agrees with the data reported by different researchers (Hameed 2009; Zhao *et al.* 2018). For this reason, the adsorbent mass of 0.1 g was chosen for the rest of the experiments.

3.3. Sorption kinetic models

The adsorption kinetics is important for the development of the adsorption system design, which determines the time required for reaching the equilibrium for the adsorption process (Rangan Sahoo & Prelot 2020). Several models describing the diffusion of solutes at the surface and in the pores of adsorbent have been developed to explain the adsorption kinetics. The pseudo-first-order, pseudo-second-order, Elovich, and intraparticle diffusion models are used in this study to examine the adsorption rates of CR onto NC.

3.3.1. Pseudo-first-order model

The Lagergreen pseudo-first-order model is based on the assumption that the rate of change of solute uptake with time is directly proportional to the difference at saturated concentration and the amount of solid uptake with time (Lagergen 1898). This is generally applicable over the initial stage of adsorption and the nonlinear form of the model is given by:

$$log(q_e - q_t) = log\, q_e - \frac{k_1}{2.303} \times t \tag{2}$$

where q_e (mg/g) and q_t (mg/g) are the amounts of the amount adsorbed at equilibrium and at time t; k_1 (min^{-1}) the rate constant in the pseudo-first-order model determined by plotting *Log* $(q_e - q_t)$ versus t.

3.3.2. Pseudo-second-order model

The pseudo-second-order kinetic model was initially proposed by Ho & McKay (1998). The model is based on the assumption that the rate-limiting step is chemical sorption or chemisorption and predicts the behavior over the whole adsorption range,

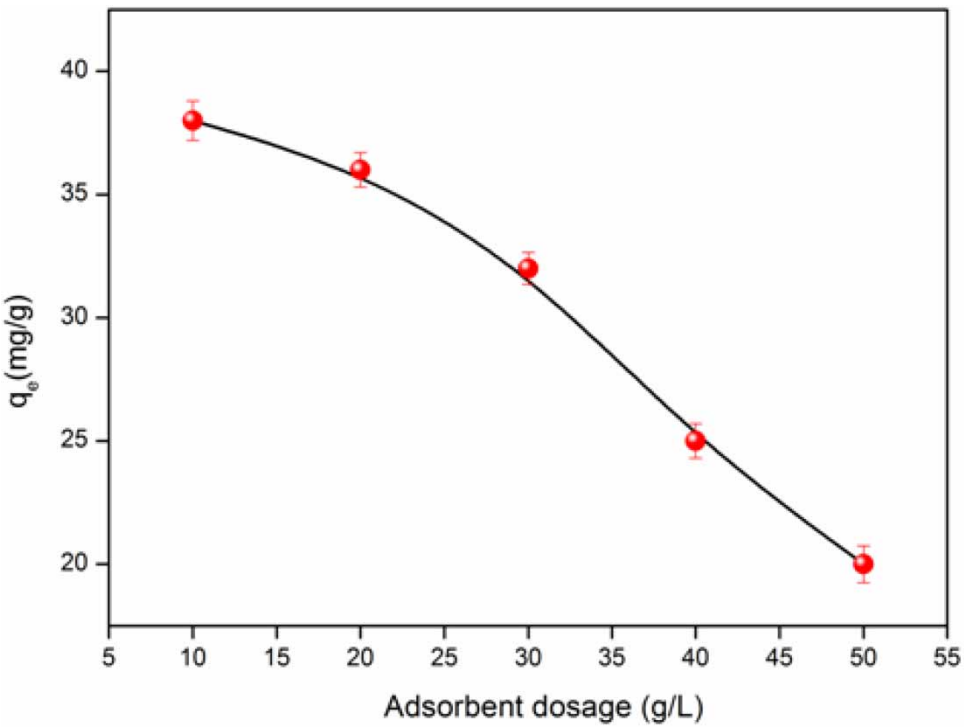

Figure 9 | Influence of the adsorbent dose on CR adsorption amount (C_i =100 mg/L, agitation speed V = 600 trs/min, pH = 2, T = 25 °C, and t = 60 min).

involving sharing or exchange of electrons between the solute and the sorbent. It assumes the adsorption of one adsorbate molecule onto two active sites on the sorbent surface; the nonlinear form of the model is given by:

$$\frac{t}{q_t} = \frac{1}{K_2 \cdot q_e^2} + \frac{1}{q_e} \cdot t \tag{3}$$

where K_2 (g /mg min) is the pseudo-second-order rate constant and q_e determined by plotting t/q_t versus t (Figure 10). The initial adsorbent rate h (mg/g min) is determined from K_2 and q_e:

$$h = K_2 q_e^2 \tag{4}$$

3.3.3. Elovich model

The Elovich model is often used to interpret the adsorption kinetics and successfully describes second-order model assuming that the surface is energetically heterogeneous (Cheung *et al.* 2001):

$$q_t = \left(\frac{1}{\beta}\right) \ln \alpha \cdot \beta + \left(\frac{1}{\beta}\right) \ln t \tag{5}$$

where α (mg/gmin) is the initial adsorption rate and β (mg/g) the relationship between the degree of surface coverage and the activation energy involved in the chemisorption.

3.3.4. Intraparticle diffusion model

To identify the diffusion mechanism in the adsorption, the intraparticle mass transfer diffusion model has been proposed by Weber & Morris (1963) and the whole equation is written as follows:

$$q_t = K_{\text{in}} \sqrt{t} + C \tag{6}$$

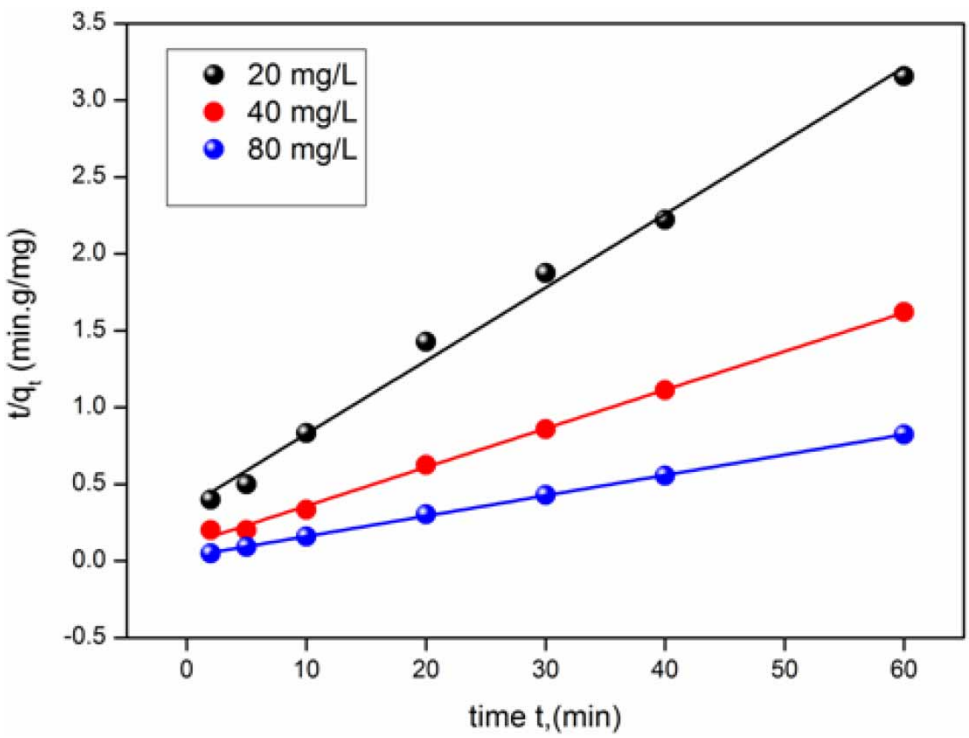

Figure 10 | Modeling of kinetics by the pseudo-second-order model.

K_{in} is the intraparticle diffusion rate (mg/gmin$^{1/2}$), q_t the amount of iodine adsorbed at time t and C (mg/g) the intercept. The constants of the various kinetic models along with the calculation of statistical errors obtained after modeling are grouped in Table 2. The relation between q_t and $t^{1/2}$ displayed a multi-linear plot (i.e., different linear stages) of the iodine experimental data, which reflects different diffusion types. The first sharp stage explains the external mass transfer of iodine from the contaminated solution to the outside surface of the developed NC adsorbent. The second and last stages reflect the pore diffusion and equilibrium phases, respectively. Consequently, the adsorption of iodine molecules on the adsorbent was directed by more than one mechanism (i.e., chemical reaction and pore diffusion are involved in the uptake of iodine by the tested adsorbent). If the intraparticle diffusion occurs, the plot q_t against $t^{0.5}$ should be linear and the line should pass by the origin, indicating that intraparticle diffusion is the only rate-limiting parameter controlling the process. Otherwise, some other mechanisms are also involved. The intercept gives an indication of the thickness of the boundary layer, i.e., the larger the intercept the greater is the boundary layer effect (Kannan & Sundaram 2001).

3.4. Adsorption isotherm models

Adsorption isotherms which describe how an adsorbate interact with adsorbent are critical in optimizing the use of adsorbents. The amount of adsorbate per unit mass of adsorbent at equilibrium q_e (mg/g) and the adsorbate equilibrium concentration, C_e (mg/L) allows plotting the adsorption isotherm, q_e versus C_e, (Figure 11). Mathematical models can be used to describe and characterize the CR adsorption. The experimental data were fitted to four common isotherm models: Langmuir, Freundlich, Temkin, and Elovich describing solid-liquid sorption of CR onto NC.

Langmuir model (Langmuir 1918) postulates the occurrence of monolayer adsorption onto fixed number of localized sites on an adsorbent surface. The model further assumes that a given adsorbent surface is composed of sites homogeneously equivalent in their enthalpies but with no subsequent movement of adsorbed molecules in the surface plane and no interactions between neighboring adsorbate molecules; the linear expression is given by:

$$\frac{1}{q_e} = \frac{1}{q_{\max}} + \frac{1}{q_{\max} \cdot K_L \cdot C_e} \tag{7}$$

$q_{\max}$ is the monolayer adsorption capacity (mg/g) while the constant K_L (L/mg) is related to the free adsorption energy. It is used to determine the dimensionless separation factor R_L and indicates the favorability of the adsorption process:

$$R_L = \frac{1}{1 + K_L \cdot C_0} \tag{8}$$

R_L indicates the type of isotherm: irreversible ($R_L = 0$), favorable ($0 < R_L < 1$), linear ($R_L = 1$) or unfavorable ($R_L > 1$). In this contribution, R_L is smaller than 1, thus confirming that the adsorption is favourable in both cases as well as the applicability of the Langmuir isotherm.

Table 2 | Pseudo-first-order and pseudo-second-order, model constants, and determination coefficients for CR adsorption onto NC

	Second-order					Pseudo-first-order			
C_0 (mg/L)	q_{ex} (mg/g)	q_{cal} (mg/g)	R^2	SSE	K_2 (g/mg.mn)	q_{cal} (mg/g)	R^2	SSE (%)	K_1 (mn^{-1})
20	19.92	20.92	0.992	0.038	0.00655	15.704	0.950	0.046	0.064
40	38.56	39.68	0.997	0.004	0.00601	25.343	0.939	0.098	0.084
80	75.15	76.9	0.999	0.0001	0.00626	40.438	0.930	0.138	0.092
	Elovich					**Diffusion**			
C_0 (mg/L)	R^2	β (g/mg)	α (mg/g.mn)	SSE		K_{in} (mg/g.mn$^{1/2}$)	R^2	C (mn$^{1/2}$)	
20	0.985	0.250	7.852	1.836		2.515	0.921	2.440	
40	0.876	0.136	26.898	54.93		4.649	0.778	7.708	
80	0.936	0.106	500.55	45.96		8.018	0.679	23.97	

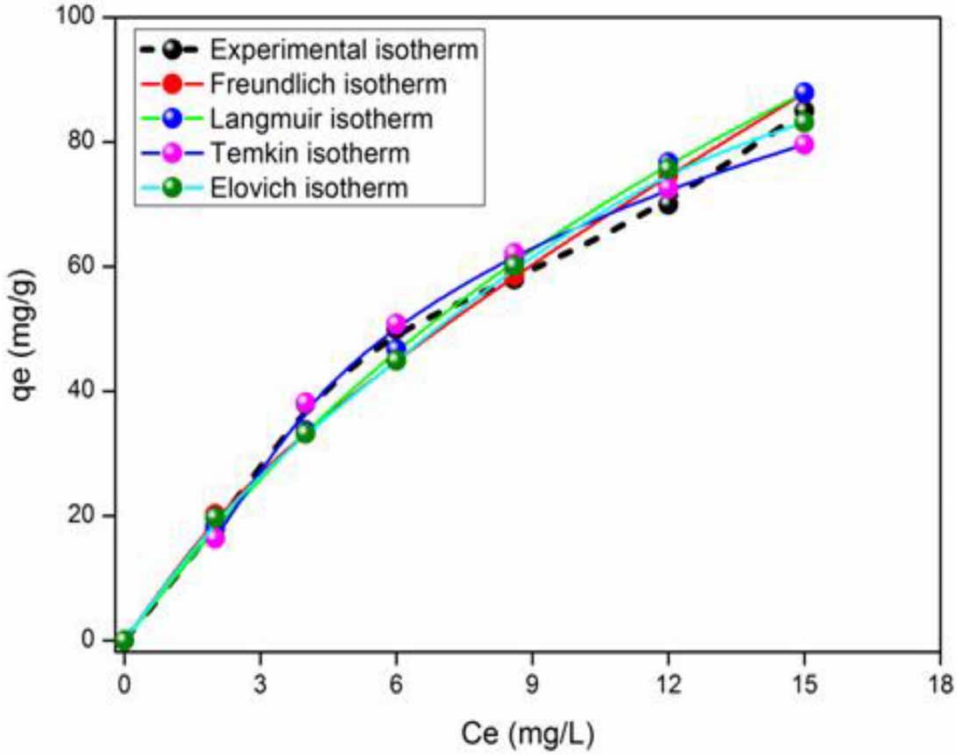

Figure 11 | Modeling of adsorption isotherms (pH = 2, adsorbent dose = 1 g/L, agitation speed $V = 600$ trs/min, and $T = 25$ °C).

Freundlich's model (Temkin & Pyzhev 1940) is based on the formation of unlimited multilayer's of adsorbed species, with an infinite surface coverage predicted on a heterogeneous surface. The enthalpies of the adsorbent surface sites follow a logarithmic distribution, where the higher energy sites with a greater affinity for the adsorbate are occupied first, followed by the lower energy sites. The sorption process is summed across sites, and the linear expression of the Freundlich model is given by:

$$\ln q_e = \ln K_F + \frac{1}{n}\ln C_e \tag{9}$$

K_F (L/g) and n are the Freundlich constants, related, respectively, to the capacity of adsorption and favorability of adsorption; the plot lnq_e versus lnC_e enables us to extract the constants K_F and n. The latter indicates the favorability of the adsorption process. When the value is between 2 and 10, favorable adsorption is expected, while n-value less than unity indicates poor sorption characteristics.

Similar to Freundlich's model, Temkin's model (Freundlich 1906) postulates the heterogeneity of an adsorbent surface, whose adsorption energy distribution is linear; the nonlinear form is given by:

$$q_e = B_T \ln C_e + B_T \ln A_T = \frac{Q_m \cdot R \cdot T}{\Delta Q}\ln C_e + \frac{Q_m \cdot R \cdot T}{\Delta Q}\ln A_T \tag{10}$$

$$B_T = \frac{Q_m \cdot R \cdot T}{\Delta Q}$$

where ΔQ (J/mol) is the adsorption energy change, $q_{\max}$ (mg/g) the maximum adsorption capacity. T (K) is the absolute temperature and R is the universal gas constant. The adsorption data are analyzed according to Equation (10) and the linear plot q_e versus ln C_e permits to calculate the constants A_T and B_T.

Elovich model (Cheung *et al.* 2000) is based on the principle of the kinetic, assuming that the number of adsorption sites augments exponentially with the adsorption, thus implying a multilayer adsorption described by Equation (11):

$$\ln \frac{q_e}{C_e} = \ln (q_{\max} .K_E) - \frac{q_e}{q_{\max}} \tag{11}$$

where K_E (L/mg) is the Elovich constant at equilibrium, $q_{\max}$ (mg/g) the maximum adsorption capacity, q_e (mg/g) the adsorption capacity at equilibrium and C_e (g/L) the concentration of the adsorbate at equilibrium. The constants KE and q_e are calculated from the plot of ln(qe/Ce) versus q_e. The constants of the various models of isotherms applied as well as the calculation of statistical errors obtained after modeling are gathered in Table 3.

3.5. Thermodynamic properties modeling studies

Figure 12 shows that the adsorption is favored at high temperature, and similar results are reported in the literature for the thermal effect (Zhang *et al.* 2017; Guo *et al.* 2020). Temperature has two important effects, known to increase the energy of mobility and the rate of diffusion of iodine ions through the boundary layer and into the internal pores of the adsorbent, due to the decrease of the viscosity of the solution (Onal *et al.* 2007). The rates of most chemical reactions increase markedly with raising the temperature, typically doubling with a temperature rise of few degrees Kelvin. The thermodynamic properties were investigated to determine whether the adsorption process occurred spontaneously. The thermodynamic parameters, namely, standard enthalpy (ΔH^0, kJ/mol), standard entropy (ΔS^0, J/mol K), and standard free energy (ΔG^0, kJ/mol), were calculated using the following equations:

$$\Delta G^0 = \Delta H^0 - T\Delta S^0 \tag{12}$$

$$\Delta G^0 = -RT \ln K_0 \tag{13}$$

$$\ln K_0 = -\frac{\Delta H^0}{RT} + \frac{\Delta S^0}{R} \tag{14}$$

where K_0 is the apparent equilibrium constant. ΔH^0 and ΔS^0 obtained from the slope and intercept of the plots lnK_0 versus $1/T$ (Figure 13) and the free energy change ΔG^0 is calculated from Equation (14), all thermodynamic parameters are listed in Table 4. The thermodynamic parameters showed that a negative value of ΔG^0 and positive of ΔH^0 confirms the spontaneous and endothermic nature of the adsorption of iodine onto (NC). The positive entropy ΔS^0 indicates an increased randomness of the solid-liquid interface during the adsorption process.

3.6. Reusability of NC adsorbent

The viability of any adsorbent on a commercial scale depends primarily on its recyclability. The reactivation of active sites of the adsorbent surface from adsorbed molecules is a basic step to enter new adsorption cycle. In this study, the adsorbent NC washed by acidic solvent followed by drying in incubator at 60 °C for 1 h to desorbed CR molecules from adsorbent to the solution. The removal percentages are given during three continuous cycles. The diagram showed the deactivation effect of adsorption efficiency from 55.5% in the first cycle to 25.3% at three cycles. The decreasing in the adsorption efficiency is due to the partial coverage of NC active sites by the CR molecules which are not easy to desorb from the adsorbent surface.

Table 3 | Parameters of the adsorption isotherms for CR dye onto NC

25 °C	Langmuir	Freundlich	Temkin	Elovich
K_L	0.047 L/mg	$1/n$: 0.728	B: 31.369	K_E: 0.099 L/mg
$q_{\max}$	212.766 mg/g	n: 1.374	A_T: 0.843 L/mg	$q_{\max}$: 116.279 mg/g
		K_F: 12.23 mg/g	ΔQ: 16.816 KJ/mol	
R^2	0.985	0.963	0.974	0.775
RSE	0.0001	0.045	56.38	0.045

RSE, Residual Sum of Errors; R^2, determination coefficient; ΔQ, Temkin Energy.

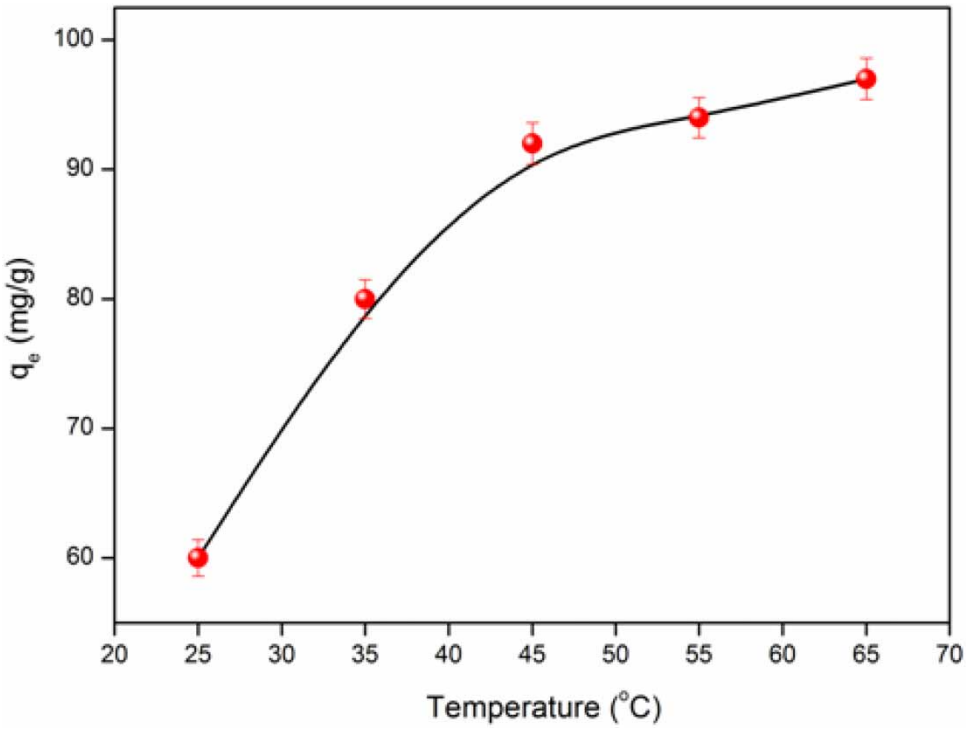

Figure 12 | Effect of temperature on the adsorption amount of CR onto NC (C_i =100 mg/L, adsorbent dose = 1 g/L, agitation speed V = 600 trs/min, pH = 2, and t = 60 min).

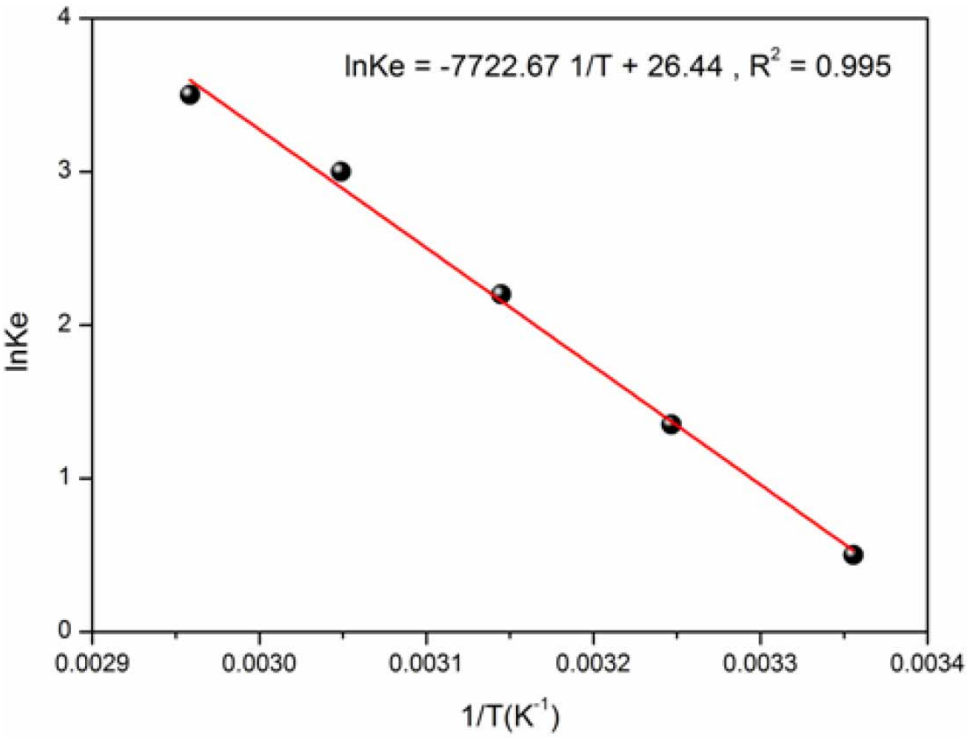

Figure 13 | The determination of thermodynamic parameters.

Table 4 | Thermodynamic functions ΔG^0, ΔS^0 and ΔH^0 of CR adsorbed onto NC

T (K)	$1/T$ (K^{-1})	LnK	ΔH^0 (KJ/mol)	ΔS^0 (kJ/K.mol)	ΔG^0 (kJ/mol)
298	0.00336	0.5	64.175	0.2197	−1.087
308	0.00325	1.35			−3.492
318	0.00314	2.2			−5.690
328	0.00305	3.0			−7.886
338	0.00296	3.5			−10.081

Table 5 | Comparison of maximum adsorption capacities for CR dye with literature data

Adsorbent	q_{max} (mg/g)	Reference
Activated carbon (ASAC)	23.42	Namasiva Yam & Arasi (1997)
Waste red mud	4.04	Gupta *et al.* (1990)
Mixed adsorbent fly ash and coal	44.00	Namasivayam *et al.* (1996)
Waste orange peel	22.44	Namasivayam & Kanchana (1993)
Waste banana pith	9.50	Lian *et al.* (2009)
Ca-Bentonite	107.41	Namasivayam & Kavitha (2002)
Coir pith	6.70	Namasivayam *et al.* (1994)
Waste Fe(III)/Cr(III) Hydroxyde	1.01	Bouchamel *et al.* (2011)
Activated carbon (Zn CO_2) 800	35.21	Sumanjit *et al.* (2013)
Activated carbon (Zn 600, CO_2 800)	30.22	Sumanjit *et al.* (2013)
Ground nut shells charcoal	117.6	Cotoruelo *et al.* (2010)
Eichhonia charcoal	56.80	Cotoruelo *et al.* (2010)
Lignin-based activated carbons	812.5	Ozman & Yilmaz (2007)
Apricot stone activated carbon (ASAC)	32.852	Abbas & Trari (2015)
TiO_2 semiconductor	152.0	Abbas (2020)
Natural clay (NC)	**212.766**	**This study**

3.7. Comparison of NC with other existing adsorbents

In order to demonstrate the effectiveness of the adsorbent (NC) for the adsorption of CR in an aqueous medium, the results obtained were compared with other adsorbents reported in the open literature (Table 5). The maximum adsorption capacity is used as a comparative parameter. It should be noted that the maximum absorption capacity obtained for NC is satisfactory compared to other adsorbents, this result shows that our adsorbent is a good attractive candidate for its contribution in the treatment of industrial effluents. Combination tests of this adsorbent with TiO_2, SnO_2, and $CaTiO_3$ as semiconducting photocatalysts are possible for the development of hybrid compounds with applications in heterogeneous photocatalysis.

4. CONCLUSION

The experimental study on the utilization of NC was used to remove CR from aqueous solutions. The influence of different physical parameters such as pH, initial iodine concentration, contact time, adsorbent dose, agitation speed, and temperature was examined. The adsorption capacity increased with augmenting the initial CR concentration, time and the maximum adsorption was obtained at the optimal pH of ~2. The kinetics of CR removal showed an optimum contact time of 40 min via a two-stage adsorption profile with an initial fast step followed by a slow equilibrium. The adsorption kinetic follows a pseudo-second-order model with a determination coefficient of R^2 close to unity, which relies on the assumption that the chemisorption is the rate-limiting step where the CR ions are chemically bonded to the adsorbent surface and tend to find sites which maximize their coordination number with the surface. The equilibrium adsorption data were analyzed, indicating that the Langmuir model provides the best correlation (212.766 mg/g at 25 °C) with a homogenous adsorption of CR on monolayer NC sorption sites. The adsorption isotherms at different temperatures have been used for the determination of the

free energy ΔG^0, enthalpy and entropy. The negative ΔG^0 and positive ΔH^0 indicated a spontaneous and endothermic nature of the reaction. The comparison of the adsorption capacity of the prepared adsorbent with the literature showed its attractive properties from industrial and economic interests. The combination of high adsorption capacity and fast equilibrium suggests that this material is a noteworthy candidate for the wastewater treatment.

DATA AVAILABILITY STATEMENT

All relevant data are included in the paper or its Supplementary Information.

CONFLICT OF INTEREST

The authors declare there is no conflict.

REFERENCES

Abbas, M. 2020 Experimental investigation of titanium dioxide as an adsorbent to remove Congo Red (CR) from aqueous solution – Equilibrium and kinetics modeling. *Journal of Water and Reuse Desalination* **10** (3), 251–266.

Abbas, M. 2021 Mass transfer processes in the adsorption of lead (Pb^{2+}) by apricot stone activated carbon (ASAC) – Isotherms modeling and thermodynamic study. *Protection of Metals and Physical Chemistry of Surfaces* **57** (4), 687–698.

Abbas, M. 2022 Removal of basic fuschine in aqueous solution by adsorption process onto Prunus Ceracefura (LPC) kinetic, isotherm modeling and thermodynamic study. *Journal of Engineered Fibers and Fabrics* **17** (1–10). https://doi.org/10.1177/1558925021991854.

Abbas, M. & Trari, M. 2015 Kinetic, equilibrium and thermodynamic study on the removal of Congo red from aqueous solutions by adsorption onto apricot stone. *Process Safety and Environmental Protection* **98**, 424–436.

Abbas, M. & Trari, M. 2020a Removal of Methylene Blue (MB) in aqueous solution by economic adsorbent derived from Apricot Stone Activated Carbon (ASAC). *Fibers and Polymers* **21** (4), 810–820.

Abbas, M. & Trari, M. 2020b Photocatalytic degradation of Asucryl Red (GRL) in aqueous medium on heat-treated TiO_2 powder – Effect of analytical parameters and kinetic modeling. *Desalination and Water Treatment* **180**, 398–404.

Abbas, M., Harrache, Z. & Trari, M. 2019 Removal of Gentian Violet (GV) in aqueous solution by activated carbon equilibrium, kinetics, and thermodynamic study. *Adsorption Science & Technology* **37** (7–8), 566–589.

Abbas, M., Harrache, Z. & Trari, M. 2020 Mass-transfer processes in the adsorption of Crystal Violet (CV) by activated carbon derived from pomegranate peels: Kinetics and thermodynamic studies. *Journal of Engineered Fibers and Fabrics* **15** (1), 1–11.

Bouchamel, N., Merzougui, Z. & Addoun, F. 2011 Adsorption en milieu aqueux de deux colorants sur Charbons Actifs a base de noyaux de date. *Journal Société Algérienne de Chimie* **21** (1), 1–14.

Brew, D. R. M. & Glasser, F. P. 2005 Synthesis and characterisation of magnesium silicate hydrate gels. *Cement and Concrete Research.* **35** (1), 85–98.

Chen, Z., Chen, H., Pan, X., Lin, Z. & Guan, X. 2015 Investigation of methylene blue biosorption and biodegradation by Bacillus thuringiensis. *Water, Air, & Soil Pollution* **3**, 226.

Cheung, C. W., Porter, J. F. & McKay, G. 2000 Elovich equation and modified second-order equation for sorption of cadmium ions onto bone char. *Journal of Chemical Technology and Biotechnology* **75** (N11), 963–970.

Cheung, C. W., Porter, J. F. & Mckay, G. 2001 Sorption kinetic analysis for the removal of cadmium ions from effluents using bone char. *Water Research* **35**, 605–612.

Christidis, G. E. & Mitsis, I. 2006 A new Ni-rich Saponite from the ophiolites complex of Othrys, Central Greece. *Clays and Clay Minerals* **54**, 653–666.

Cotoruelo, L. M., Marqués, M. D., Díaz, F. J., Rodríguez-Mirasol, J., Rodríguez, J. J. & Cordero, T. 2010 Equilibrium and kinetic study of Congo red adsorption onto lignin-based activated carbons. *Transport in Porous Media* **83**, 83573–83590.

Elnahas, M. O., Hou, L., Wall, J. D. & Majumder, E. W. 2021 Bioremediation potential of Streptomyces sp. MOE6 for toxic metals and oil. *Polysaccharides* **2**, 47–68.

Freundlich, H. 1906 Concerning adsorption in solutions. *Z. Phys. Chem. Stoch.* **57**, 385–470.

Guo, F., Jiang, X., Li, X., Jia, X., Liang, S. & Qian, L. 2020 Synthesis of MgO/Fe3O4 nanoparticles embedded activated carbon from biomass for high-efficient adsorption of malachite green. *Materials Chemistry and Physics* **240**, 122240.

Gupta, G. S., Prasad, G. & Sing, V. N. 1990 Removal of Chrom dye from aqueous solution by mixed adsorbents: Fly ash coal. *Water Research* **24**, 45–50.

Hameed, B. H. 2009 Spent tea leaves: a new non-conventional and low cost adsorbent for removal of basic dye from aqueous solutions. *Journal of Hazardous Materials* **161**, 753–759.

Ho, Y. S. & McKay, G. 1998 Kinetic models for the sorption of dye from aqueous solution by wood. *Journal of Environnement Science Health B* **76** (4), 183–191.

Homaeigohar, S. 2020 The nanosized dye adsorbents for water treatment. *Nanomaterials* **10**, 295.

Ismail, W. N. W., Syah, M. I. A. I., Muhet, N. H. A., Bakar, N. H. A., Yusop, H. M. & Samah, N. A. 2022 Adsorption behavior of heavy metal ions by hybrid inulin-TEOS for water treatment. *Civil Engineering Journal* **8** (09), 1787–1798.

Kannan, K. & Sundaram, M. 2001 Kinetics and mechanism of removal of methylene blue by adsorption on various carbons, a comparative study. *Dyes Pigment* **51**, 25–40.

Krishna Moorthy, A., Govindarajan Rathi, B., Shukla, S. P., Kumar, K. & Shree Bharti, V. 2021 Acute toxicity of textile dye Methylene blue on growth and metabolism of selected freshwater microalgae. *Environmental Toxicology and Pharmacology* **82**, 103552.

Lagergen, S. 1898 Zur theorie der sogenannten adsorption geloster stoffe. *Kungliga Svenska Vetenskapsakademiens Handlingar* **24** (4), 1–39.

Langmuir, I. 1918 The adsorption of gases on plane surfaces of glass, mica and platinum. *Journal of American. Chemical Society* **40**, 1361–1403.

Lian, L., Guo, L. p. & Guo, C. 2009 Adsorption of Congo Red from aqueous solutions onto Ca-bentonite. *Journal of Hazardouz Materials* **161** (1), 126–131.

Mall, I. D., Srivastava, V. C., Agarwal, N. K. & Mishra, I. M. 2005 Removal of Congo red from aqueous solution by Bagasse fly ash and activated carbon: Kinetic study and equilibrium isotherm analyses. *Chemosphere* **61** (4), 492–501.

Matei, C., Berger, D., Dumbrava, A., Radu, M. D. & Gheorghe, E. 2020 Calcium carbonate as silver carrier in composite materials obtained in green seaweed extract with topical applications. *Journal of Sol-Gel Science and Technology* **93** (2), 315–323.

Namasiva Yam, C. & Arasi, D. J. S. E. 1997 Removal of Congo Red from wastewater by adsorption onto waste red mud. *Chemosphere* **34** (2), 401–417.

Namasivayam, C. & Kanchana, N. 1993 Removal of Congo red from aqueous solutions by cellulosic waste banana pith, pertanica. *Journal of Science Technology* **1**, 32–42.

Namasivayam, C. & Kavitha, D. 2002 Removal of dyes from aqueous solutions by adsorption onto activated carbon prepared from Coir Pith, an agricultural solid waste. *Deys and Pigment* **54**, 47–58.

Namasivayam, C., Jeya Kumar, R. & Yamuna, R. T. 1994 Dyes removal from wastewater by adsorption on waste Fe(III)/Cr(III). *Waste Management* **14**, 643–648.

Namasivayam, C., Muniasamy, N., Gay thri, K., Rani, M. & Ranganathan, K. 1996 Removal of dyes from aqueous solutions by cellulosic waste orange peel. *Bioresource Technology* **57** (1), 37–43.

Nasuha, N. & Hameed, B. H. 2011 Adsorption of methylene blue from aqueous solution onto NaOH-modified rejected tea. *Chemical Engineering Journal* **166** (2), 783–786.

Omar, H., El-Gendy, A. & Al-Ahmary, K. 2018 Bioremoval of toxic dye by using different marine macroalgae. *Turkish Journal of Botany* **42**, 15–27.

Onal, Y., Akmil-Basar, C. & Sarıcı-Ozdemir, C. 2007 Investigation kinetics mechanisms of adsorption malachite green onto activated carbon. *Journal of Hazardous Materials* **146**, 194–120.

Ozman, E. Y. & Yilmaz, M. 2007 Use of β-cyclodextrin and starch based polymer for sorption of Congo Red from aqueous solutions. *Journal of Hazardous Materialss* **148**, 303–310.

Rangan Sahoo, T. & Prelot, B. 2020 Adsorption processes for the removal of contaminants from wastewater: The perspective role of nanomaterials and nanotechnology. In: (Bonelli, B., Freyria, F. S., Rossetti, I. & Sethi, R. eds). *Nanomaterials for the Detection and Removal of Wastewater Pollutants, Micro and Nano Technologies*. Elsevier, The Netherlands, 161–222.

Reddad, Z., Gerente, C., Andres, Y. & Le Cloirec, P. 2002 Adsorption of several metal ions onto a low-cost biosorbent: Kinetic and equilibrium studies. *Environmental Science and Technoogy.* **36** (9), 2067–2073.

Sumanjit, K., Seema, R. & Rakesh Kumar, M. 2013 Adsorption kinetics for the removal of hazardous dey Congo Red Biowaste Materials as adsorbents, Hindawi Publishing Corporation. *Journal of Chemistry* **2013**, 1–12. https://doi.org/10.1155/2013/628582.

Takhashi, N., Tanaka, M., Satoh, T. & Endo, T. 1994 Study of synthetic clay miner III. Synthesis and characterization of 2-dimensional talc. *Bulletin of the Chemical Societ of Japan* **67**, 2463–2467.

Temkin, M. & Pyzhev, V. 1940 Kinetics of ammonia synthesis on promoted iron catalysts. *ActaPhysicochim. URSS* **12**, 327–356.

Weber, W. J. & Morris, J. C. 1963 Kinetics of adsorption on carbon from solution. *Journal of the Sanitary Engineering Division; American Society Civil Engineering* **8**, 31–60.

Yandri, Y., Tiarsa, E. R., Suhartati, T., Irawan, B. & Hadi, S. 2023 Immobilization and stabilization of Aspergillus Fumigatus α-Amylase by adsorption on a Chitin. *Emerging Science Journal* **7** (1), 77–89.

Yeniyol, M. 2020 Transformation of Magnesite to Sepiolite and Stevensite: Characteristics an genesis (Cayirbagi, Konya, Turkey). *Clays and Clay Minerals* **68** (4), 347–360.

Yu, K. L., Lee, X. J., Ong, H. C., Chen, W. H., Chang, J. S., Lin, C. S., Show, P. L. & Ling, T. C. 2021 Adsorptive removal of cationic methylene blue and anionic Congo red dyes using wet-torrefied microalgal biochar: Equilibrium, kinetic and mechanism modeling. *Environmental Pollution* **272**, 115986.

Zhang, T., Yue, X., Gao, L., Qiu, F., Xu, J., Rong, J. & Pan, J. 2017 Hierarchically porous bismuth oxide/layered double hydroxide composites: Preparation, characterization and iodine adsorption. *Journal of Cleaner Production* **144**, 220–227.

Zhao, Z., Yanhui, L., Du, Q. & Li, Q. 2018 Adsorption of Congo red from aqueous solutions by porous soybean curd Xerogels. *Polish Journal of Chemical Technology* **20** (3), 95–102.

First received 25 February 2023; accepted in revised form 29 July 2023. Available online 9 August 2023